INDEX COPERNICUS INTERNATIONAL



Bio-Algorithms and Med-Systems

WWW.BAMSJOURNAL.COM ISSN: 1896-530X

ORIGINAL ARTICLE

Received: 20.08.2024
Accepted: 14.11.2024
Published: 17.12.2024

CITE THIS ARTICLE AS:
Romanchek GR, Shoop G, Kupinski MA, Kuo PH, King M, Furenlid LR, Abbaszadeh S, "Investigation of Quantum Entanglement Information for $\beta^+\gamma$ Coincidences," Bio-Algorithms and Med-Systems vol. 20, special issue, pp. 27-34, 2024, DOI: 10.5604/01.3001.0054.9079

AUTHORS' CONTRIBUTION:
A. Conceptualization
B. Data Curation
C. Formal Analysis
D. Funding Acquisition
E. Investigation
F. Methodology
G. Project Administration
H. Resources
I. Software
J. Supervision
K. Validation
L. Visualization
M. Writing – Original Draft
N. Writing – Review & Editing

CORRESPONDING AUTHOR:
Shiva Abbaszadeh; Department of Electrical and Computer Engineering, Baskin School of Engineering, University of California Santa Cruz, Santa Cruz, CA, USA;
E-mail: sabbasza@ucsc.edu

COPYRIGHT:
Some rights reserved: Jagiellonian University Medical College. Published by Index Copernicus Sp. z o. o.

OPEN ACCESS:
The content of the journal „Bio-Algorithms and Med-Systems" is circulated on the basis of the Open Access which means free and limitless access to scientific data.

CREATIVE COMMONS CC BY:
Attribution. It is free to copy, distribute, present and perform the copyrighted work and derivative works developed from it, provided that the name of the original author is cited.

Investigation of Quantum Entanglement Information for $\beta^+\gamma$ Coincidences

Gregory R. Romanchek[1,2ABCEFIKLMN], **Greyson Shoop**[2CEM], **Matthew A. Kupinski**[3N], **Phillip H. Kuo**[3N], **Michael King**[4N], **Lars R. Furenlid**[3N], **Shiva Abbaszadeh**[2ADGHMN]

[1]Department of Nuclear, Plasma, and Radiological Engineering, Grainger College of Engineering, University of Illinois at Urbana-Champaign, Urbana, IL, USA
[2]Department of Electrical and Computer Engineering, Baskin School of Engineering, University of California Santa Cruz, Santa Cruz, CA, USA
[3]Deptartment of Medical Imaging, Wynat College of Optical Sciences, University of Arizona, Tucson, AZ, USA
[4]Deptartment of Radiology, T. H. Chan Medical School, University of Massachusetts, Worcester, MA, USA

ABSTRACT

Objective: We assess the viability of using quantum entanglement (QE) information for improving event classification in a combined PET-Compton Camera (PET-CC) system, particularly in the potential for distinguishing true positron annihilation events from Random events due to prompt gamma contamination for β^+ and γ emitting isotopes.
Methods: Monte Carlo GATE simulations were performed to evaluate the sensitivity and accuracy of event classification in various scenarios using ground truth data, including standard PET events and Compton Camera interactions. QE-sensitive data subsets were identified and filtered based on either polar scattering angles (θ) or the energy of the initial Compton scatter (E_C). The enhancement ratio – ratio of the difference of azimuthal scattering at $\Delta\phi = 90°$ and $0°$ – and fraction of post-filter Trues were used as metrics.
Results: The simulations showed that QE information could assist in resolving energy ambiguities, particularly in cases where prompt gamma emissions complicate event pairing. Filtering based on E_C provided a higher enhancement ratio ($R \approx 1.8$) compared to θ-based filtering ($R \approx 1.4$), indicating better discrimination between True and Random events. The ratio of Trues to Total events passing the E_C filter (0.837) greatly improved upon that of the θ-based filter (0.541).
Conclusions: Our results suggest that energy-based filtering is more effective in leveraging QE information, but further refinement of filtering algorithms is needed to fully realize its benefits. While QE has the potential to improve event classification in PET-CC systems for a few coincidence cases, further studies are needed to utilize this paradigm in image formation.

KEYWORDS

PET Imaging, Quantum Entanglement, Compton Camera, Monte Carlo Simulation, CZT

BRIEF DESCRIPTION OF THE WORK

This study addresses the challenge of accurately distinguishing true positron annihilation events from Random events caused by prompt gamma emissions in combined PET-Compton Camera (PET-CC) systems targeting isotopes with dual β^+ and γ emission. Improving event classification in these systems is crucial for enhancing the accuracy of imaging in clinical diagnostics and treatment planning, particularly in cases involving complex multi-isotope studies.

LIST OF ABBREVIATIONS

2P – 2-Panel PET Scanner
C – Compton scatter
CC – Compton camera
COR – cone of response
DCSc – Compton scattering event
E_c – initial Compton scatter
FOV – field-of-view
GATE – Geant4 Application for Emission Tomography
LOR – lines of response
MIPEs – multiple interaction photon events
P – photoelectric absorption
PET – Positron Emission Tomography
PET-CC – PET-Compton Camera
QE – quantum entanglement
R – ratio

INTRODUCTION

Positron Emission Tomography (PET) is an important imaging modality for clinical diagnostics and treatment planning, for it provides insights into the metabolic and functional processes of various diseases, enabling early detection, accurate staging and effective monitoring of therapeutic responses. It uses the back-to-back 511 keV positron annihilation photons to create lines of response (LOR) for localizing the tracer distribution in a subject. PET is highly sensitive and can detect very low levels of radiotracer concentrations. However, the spatial resolution of PET systems is limited by the range that positrons (β^+) travel in tissue after emission from the radiotracer and before annihilating with electrons to produce two 511 KeV photons. This positron range causes a blurring effect, which can limit the precise localization of metabolic activity. This effect is particularly significant for isotopes that emit positrons with higher kinetic energy, as the positrons travel further before annihilation [1]. Combining PET and Compton camera (CC) in a single system is motivated by the complementary strengths of each imaging modality to enhance the sensitivity and spatial resolution in nuclear medicine imaging [2]. A combined PET-CC system enables imaging radioisotopes undergoing $\beta^+\gamma$ decay, where single emission gammas are released, in addition to a β^+. The emission of prompt gamma rays (γ_{prompt}) during $\beta^+\gamma$ decay originates directly from the radioisotope rather than from the β^+. Consequently, using a CC to capture the scattering of the γ_{prompt} allows for the projection of cone of response (COR), which is not affected by the positron range effects that LORs in PET are subject to. Further, prompt gamma signals have the potential to enable multi-tracer PET imaging [2–5]. The energy and timing signatures of prompt gammas are distinctive to specific radioisotopes and can be used to assign correlated annihilation detection events to individual tracers in multi-tracer studies. Incorporation of a prompt gamma signal also allows for positronium lifetime imaging applications, wherein the detection of the prompt gamma corresponds with the emission time of the positron, and the detection of the annihilation photons corresponds with positronium decay [6, 7]. The time resolution (sub-ns) required for such an application, however, is beyond the capabilities of the presented system and so is not currently a consideration of this work.

Multiple groups are working on instrumentation to enable high--performance $\beta^+\gamma$ imaging. Different architectures and detector configurations have been proposed either by inserting a scattering detector ring between the cylindrical PET detectors [8] or by utilizing detector modules capable of coincidence detection of $\beta^+\gamma$, such as liquid xenon detectors [9] and edge-on Cadmium zinc telluride [10]. Sorting and pairing the events to accurately define LOR from annihilation photon pairs and the COR from the prompt gamma rays present additional complications that did not exist in the conventional PET scanners. These complications depend on the specifics of detector technology, detector configuration, geometry and the energy of the scatter profile of the γ_{prompt} compared to the 511 keV energy window. One area of interest that has not been investigated to tackle the sorting complications in $\beta^+\gamma$ is utilizing the quantum entanglement (QE) of photons resulting from para--positronium annihilation.

The existence of entangled particles and the properties of entangled photons from β^+ annihilation has been extensively researched since the 1940s [11–13]. In recent years, physicists have observed that such entanglement is manifested via the Compton scattering kinematics of positron annihilation photons and investigated its application for the purpose of improving PET imaging [14–19]. In order to capture the entangled Compton scattering kinematics, the simultaneous detection of the scattering of annihilation photons in what is known as a double Compton scattering event (DCSc) is required. DCSc constitutes a detection event in which the first interaction of both annihilation photons within the detector system is a Compton scatter and is followed by a secondary interaction (typically photoelectric absorption) so that scattering vectors can be extracted. Through the detection of DCSc events, the energy and measured positional coordinates allow for the computation of the polar (θ) and azimuthal (ϕ) scattering angles relative to the axis defined by the LOR. It has been shown that given two DCSc photons, each with their respective θ_1, θ_2, ϕ_1, and ϕ_2, when observing photons with $\theta \approx 81.7°$, the distribution of computed $\Delta\phi$ is maximum, at $\Delta\phi = \pm 90°$. This distribution is known as the enhancement ratio (R) and has a theoretical maximum of $R \approx 2.84$, meaning that when two entangled photons are detected

in a DCSc event, they have a maximum occurrence of scattering on orthogonal planes. This description of enhancement pertains to that of a positron and unbound electron in vacuum. Of note, enhancement strength may weaken with bound electrons and by material type [20]. This has implications for background reduction in PET. However, to what extent the detection of entangled photons improves PET has not been widely demonstrated.

Until recently, the question of whether positron annihilation photons' scatter events before absorbing in the detector caused decoherence, thus breaking QE and, remained unresolved. If scatter events indeed resulted in decoherence, the unique scattering kinematics of QE could be leveraged to classify both scatter and random events, as neither would remain entangled. After investigation and some debate [16, 21–23], it has been determined that the magnitude of the scatter event plays a crucial role in determining whether decoherence occurs. Theoretical work supports these findings [24]. Specifically, for small deflections, entanglement is predominantly preserved. As the scatter angle increases the $\Delta\phi$ modulation weakens, evidenced by the decreasing enhancement ratio. This implies that larger scatter angles are more likely to result in decoherence. Importantly, this phenomenon does not affect the detection of Random events, as these inherently lack entanglement. Thus, while scatter events may compromise QE, depending on the angle of deflection, random events remain unaffected due to their unentangled nature.

In this work we are utilizing the distinction that random events due to contamination of γ_{prompt} lack entanglement, and we investigate whether we can leverage this information for refining the classification of events to accurately define LOR from annihilation photon pairs and the COR from the prompt gamma rays.

MATERIALS AND METHODS

GATE Simulations

To investigate the distribution of $\beta^+\gamma$ coincidence interaction mode frequencies, we performed simulations in a GATE (v9.3 [25]), a GEANT4 (v11.1.1 [26])-based Monte Carlo physics simulator for medical imaging applications. We used the emlivermore_polar GATE physics list [27] to ensure compatibility with Watts et al.'s QE-GEANT4 extension [16] and modified the underlying source code to enable QE Compton scattering kinematics in GATE [28].

We modelled a simplified Sc-44 point source. We selected Sc-44 due to the near simultaneous and high rates of β^+ (98.97%) and γ_{Prompt} (99.875%) emissions. The high energy γ_{Prompt} (1157 keV) also added ambiguity with the annihilation photons in energy--based event classification when it scatters at or below 511 keV. Our simplified source model enforced decays, always resulted in simultaneous β^+ and γ_{Prompt} dual emissions. The point source was set with a radius of 0.1 mm centered in the field-of-view (FOV) with an activity of 30 μCi and half-life of 14,290 s. We conducted a 60-s simulated scan of the described Sc-44 point source with the following modeled system and using the GATE Hits output with our in-house-events processing software.

System Description

The UCSC 2-Panel PET Scanner (2P) is an advanced imaging system designed for high-resolution studies, particularly for head and neck imaging [29–31]. It is illustrated in Fig. 1. in the GATE geometry. It comprises two 15 × 20 cm² detector panels, each containing a 5 × 30 array of 150 CZT crystals (40 × 5 × 40 mm³) arranged in an edge-on configuration to maximize system sensitivity. The adjustable 20-cm spacing between panels allows for minimizing the distance between the scanner and the imaging target.

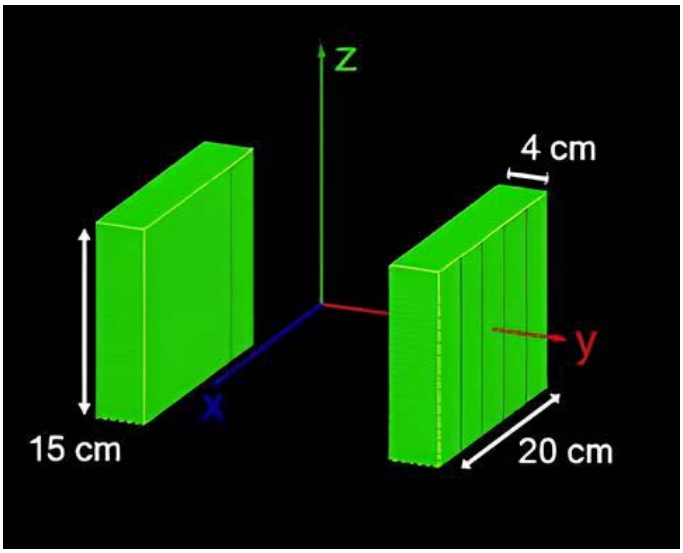

Fig. 1. Depiction of the 2-panel system defined in GATE.

The cross-strip anode-cathode design allows each CZT crystal to have 39 anodes with a 1-mm pitch and 8 cathodes with a 5-mm pitch, enabling 1 × 2.5-mm event resolution in x-y through charge, sharing information and sub-millimetre in z with the use of a cathode-to-anode ratio [32]. Further, the system has demonstrated accurate Compton scatter event recovery, with an average polar angular resolution of 0.67° for 1 × 1 × 1-mm interaction resolution and 2.65° for 1 × 3 × 1-mm interaction resolution, ensuring sub-millimetre spatial resolution [29, 33].

Event Processing

The annihilation photons resulting from para-positronium decay ($\gamma_{Ann,1}$ and $\gamma_{Ann,2}$) and γ_{Prompt}, emitted from the same simulated Sc-44 decay event. were paired based on their ground truth GATE Hit eventIDs. Each of these photons may undergo multiple interaction photon events (MIPEs), where they interact with the detector material multiple times – such MIPEs were similarly collected for each photon using a priori simulation information. When at least two of the decay photons underwent an MIPE, their respective scattering vectors could

be extracted and used for scattering angle analysis. The frequency of decays resulting in MIPEs for more than one photon was computed.

Whether MIPE or not, the first interaction of each photon from a given decay event – either photoelectric absorption (P), Compton scatter (C) or a miss (if no interaction event occured) – was also tallied. For each Sc-44 decay event we noted the first interactions of each photon as: $\gamma_{Ann,1}$ interaction, $\gamma_{Ann,2}$ interaction, γ_{Prompt} interaction. For example, C, miss, C describes a decay event in which the $\gamma_{Ann,2}$ was not detected, while $\gamma_{Ann,1}$ and γ_{Prompt} Compton scattered as their first detection event. Note that nothing was implied about MIPE in this notation. The percentage of each first interaction group was computed.

To test methods for best selecting $\beta^+\gamma$ MIPE coincidences with the greatest QE-information, we created a synthetic dataset from the sorted GATE Hits. This synthetic dataset was created with a user-controlled Random fraction and was of greater set size than otherwise achievable only with a much longer simulation. Its construction is as follows:

We collected each Hit from all MIPEs resulting from γ_{Prompt} interactions and grouped them by their event ID. We then collected each γ_{Ann} pair in which both photons underwent MIPEs and grouped them similarly. The synthetic data set was a mix of these disjointed sets. In this work we present findings from a 50% mix: half of the coincidence pairs are Trues ($\gamma_{Ann,1}$, correctly paired with $\gamma_{Ann,2}$), while the other half of pairs are Falses/Randoms ($\gamma_{Ann,1}||\gamma_{Ann,2}$, incorrectly paired with γ_{Prompt}).

In this report we specifically refer to Randoms consequential of pairing γ_{Prompt} and γ_{Ann} together rather than pairing two uncorrelated γ_{Ann} together (as is the case for Randoms in traditional PET). The Random rate in traditional PET is proportional with the source activity. In $\beta^+\gamma$ imaging, however, as each decay produces a prompt signal that may contaminate the annihilation signal, the Random rate is dependent on the ability to distinguish γ_{Ann} from γ_{Prompt}. Consider a three-photon detection event in the 2-panel system in which a γ_{Prompt} and first γ_{Ann} are detected in one panel and the second γ_{Ann} in the other panel. It is clear that γ_{Ann} pairing must be restricted to events in different panels, as true coincidence γ_{Ann} can only interact in the same panel due to a scatter event. Thus (without any energy considerations), the lone γ_{Ann} has a 50/50 chance of being paired with either the γ_{Ann} (resulting in a True) or with the γ_{Prompt} (resulting in a Random). So, the selected 50% blend of Trues and Randoms was a representative of sampling such a case.

The synthetic data set was subject to three filters: an energy of initial Compton scatter filter, defined as $E_C \in 235 \pm 10\%$ keV; a polar scattering angle filter of $\theta \in [73.12, 91.68]°$, which corresponds to the 10% energy bounds of the E_C filter; and a combined filter of both. The purpose of these filters was to select for the subset of data for which $\Delta\phi$-dependence is strongest (QE-information at its most prominent), which occured at the polar scattering angle $\theta = 81.7°$ [11–13, 16, 19]. We leveraged classical Compton kinematics in noting that a 81.7° polar scatter from a 511 keV photon corresponded with an energy deposition of 235 keV. And so we could select for the desired DCSc using either.

RESULTS

The simulation of the 60-s scan resulted in 8.94×10^7 Hits, which constituted 7.48×10^6 MIPEs from γ_{Prompt} interactions and 5.43×10^6 double MIPE from True coincidence γ_{Ann}. A subset of the first interaction data is presented in Tab. I., showing cases of interest – omitting P, miss, miss, for example. We present the sensitivity both with respect to the total number of decays (Decays) and with respect to the total number of Decays wherein at least one of the photons hit the detector (Hits). Cases that are permutations of γ_{Ann} interactions, such as (P, C, C) *vs.* (C, P, C), are combined into one case. Cases with pairing ambiguity are marked with a "^" and result from the γ_{Prompt} depositing a confounding amount of energy – cases where energy alone cannot be used to distinguish γ_{Prompt} from γ_{Ann}. For example, if the γ_{Prompt} in case 1 deposits ~511 keV, then the γ_{Ann} cannot be paired with certainty. Some of the cases – those where MIPEs are possible – can leverage QE-information to aid in γ_{Ann} pairing and are marked with an "*".

Case 2 of Tab. I. represents standard PET (P, P, miss), with a total sensitivity of 0.464% – we can recapture the full sensitivity of (P, P, any) by summing cases 1, 2, and 10 to a total sensitivity of 0.562%. The most likely is case 7 (miss, miss, C) – the Compton camera case – with a total sensitivity of 12.304%, followed by case 4 (C, C, miss) with a total sensitivity of 9.986%. Even when γ_{Prompt} is not present, such as in case 4 (C, C, miss), ambiguity may still exist when considering a dual emission isotope. Here, as γ_{Prompt} may deposit energy lower than 511 keV, energy cannot be used alone to identify if a given coincidence is case 4 (C, C, miss) or case 9 (C, miss, C).

Case 3 is special in that it: (1) has all three photons detected, (2) is energy ambiguous ("^") and (3) is such that QE-information is relevant ("*"), as each photon can have MIPEs. With a total sensitivity of 1.995%, there is significant sensitivity to be reclaimed if a robust coincidence pairing mechanism can be found. Tab. II. summarizes subcases based on the nature of the MIPE of each photon. Subcase A places no constraints on the total number of interactions following the first and so matches that in Tab. I. Subcase B (0.923%) requires each photon to have at least two total interactions – this is relevant for extracting scattering vectors to compute the polar and azimuthal scattering angles. Subcase C (0.121%) describes the portion of subcase B events in which the energy deposited by the γ_{Prompt} makes it indistinguishable from γ_{Ann} from energy alone. Subcase C is the case wherein QE-information is most valuable for correctly pairing $\gamma_{Ann,1}$ and $\gamma_{Ann,2}$.

The enhancement factor is maximized at R = 2.84 for $\theta = 81.7°$ (for the 511 keV annihilation photons) [11–13, 16, 19]. We

Tab. I. Subset of $\beta^+\gamma$ coincidences by first interaction type.

	INTERACTION TYPE			SENSITIVITY BY (%)			
Case	$\gamma_{Ann,\,1}$	$\gamma_{Ann,\,2}$	γ_{Prompt}	Decays	Hits	Modality	Comments
1^	P	P	C	0.093	0.241	PET/CC	Range correction of PET with CC information and isotope verification.
2	P	P	miss	0.464	1.206	PET	Standard PET.
3*^	C	C	C	1.995	5.184	PET/CC	QE information useful to separate γ_{Ann} from γ_{Prompt}. Aids in isotope verification.
4*	C	C	miss	9.986	25.949	PET	QE information useful to reduce Randoms.
5^	P	C	C	0.862	2.235	PET/CC	Range correction of PET with CC information and isotope verification.
6	P	C	miss	4.300	11.175	PET	Standard PET.
7	miss	miss	C	12.304	31.973	CC	CC only.
8^	P	miss	C	0.242	0.628	CC	CC only.
9^	C	miss	C	1.024	2.661	CC	CC only.
10	P	P	P	0.005	0.012	PET	PET with isotope verification. No range correction.
11*	C	C	P	0.105	0.274	PET	QE information useful to reduce Randoms with isotope verification. No range correction.
12	P	C	P	0.046	0.118	PET	PET with isotope verification. No range correction.

* – quantum entanglement analysis

^ – scattering energy ≤511 keV window leads to ambiguity

Sensitivity by Decays: percent of total Decays.

Sensitivity by Hits: percent where at least one photon was detected.

expect that the unfiltered mixed data (50/50 Trues and Randoms) will have greatly repressed enhancement and each filter to significantly increase enhancement. Further, the Random portion of the data should have no $\Delta\phi$ dependence, as expected, because these photons have no entanglement or Random relative polarization. The True portion of the data will have the greatest $\Delta\phi$ dependence and can be used as a visual benchmark for the mixed set.

Visualization of the unfiltered data in Fig. 2A. shows weak $\Delta\phi$ dependance, with an enhancement ratio of R ≈ 1.15 for the mixed set. As expected, the Random portion of the data has no $\Delta\phi$ dependence. Filtering by the polar scattering angle θ, Fig. 2B., results in R ≈ 1.4 for the mixed set – significantly lower than the True set, with R ≈ 2.25. If we select pairs by the energy deposited in the initial Compton scatter E_C instead (Fig. 2C.), we have a mixed set yielding R ≈ 1.8 and a True set with R ≈ 2.25. The performance difference between the θ and E_C filters result from a nuance of the scatter angle (θ and ϕ) computations.

The extracted scatter vectors (and thus their angles) are dependent on the measured line of response (LOR). Random DCSc kinematics have no meaningful correlation between deposited energy and polar scattering due to their false LOR vector. True DCSc kinematics, on the other hand, follow Compton kinematics. This particularity results in a disproportionate percentage of Random

Tab. II. Subcases of case 3 in Tab. I.

		SENSITIVITY BY (%)	
SUBCASE	CASE 3 SUBCASES DESCRIPTION	DECAYS	HITS
A	Each Compton scatter was followed by any number of subsequent Hits.	1.995	5.184
B	Each Compton scatter was followed by at least one subsequent Hit.	0.923	2.397
C	Each Compton scatter was followed by at least one subsequent Hit and total energy deposited was confounding.	0.121	0.315

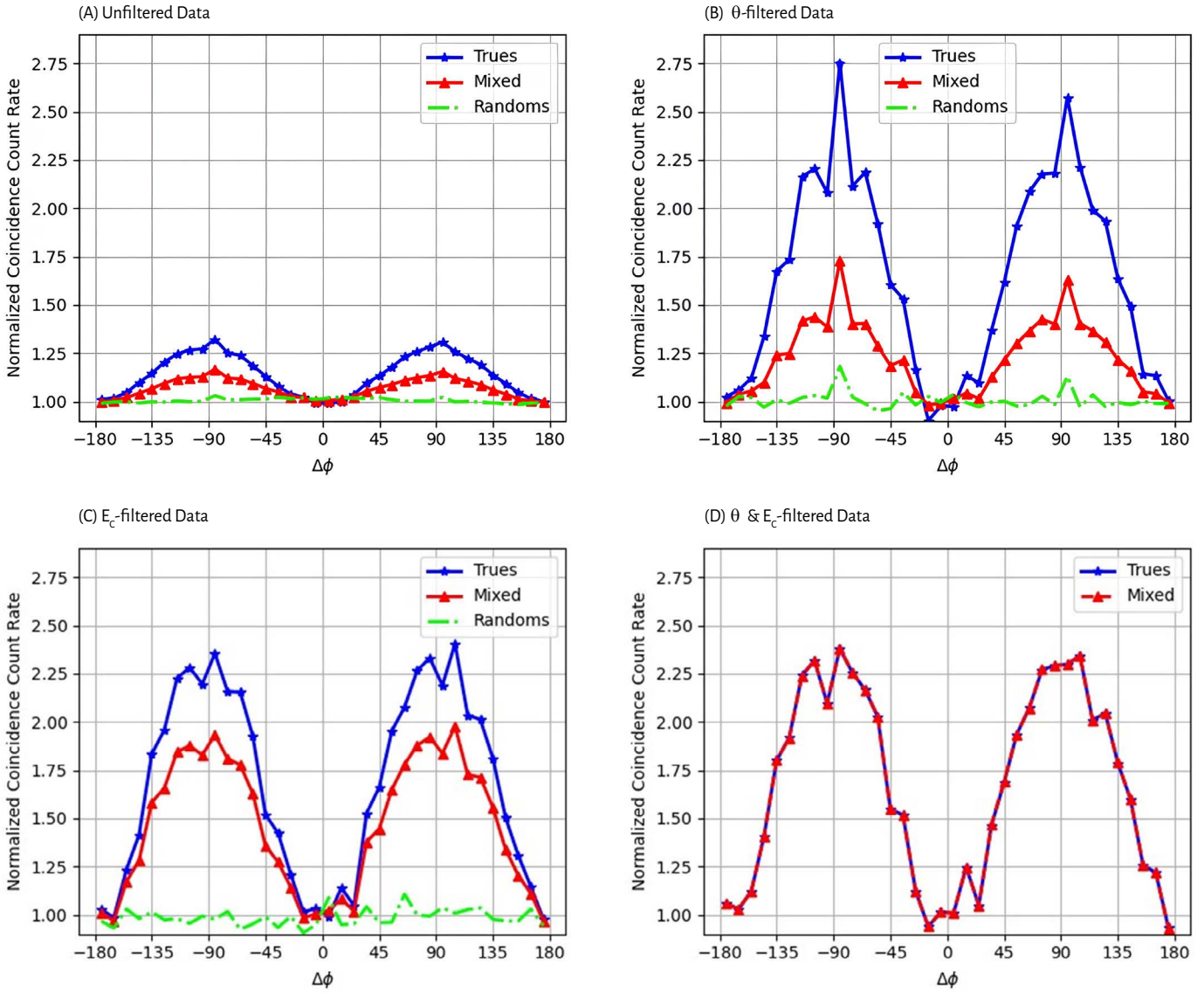

Fig. 2. Azimuthal scattering angle difference (Δφ) for each portion of the synthetic dataset: total/mixed in red (triangles), the True portion of the dataset in blue (stars), and the Random portion of the dataset in green (dashes). Each subplot displays the distribution after the given filter: (A) no filter; (B) a polar filter of $\theta \in [73.12,91.68]°$; (C) a Compton energy filter of $E_c \in 235\pm10\%$ keV and (D) both polar and Compton energy filters.

DCSc being included in the θ window by accident – they appear to scatter within $\theta \in [73.12,91.68]°$ due to false basis vectors. Meanwhile, such Randoms cannot "fake" initial energy deposition and so are more adequately selected against in an energy filter.

The quantity of data in the QE optimized subset (the $\theta \approx 81.7°$ subset) is small regardless of filter selection, with 7,381 (0.00272%) and 6,646 (0.00245%) True DCSc falling with the θ and E_c ranges from a net of 2.72×10^6 True DCSc, respectively. By contrast, the number of Randoms which survived: 6,249 (0.00230%) and 1,293 (0.00476%) True DCSc from a net of 2.72×10^6, respectively, reveals the difference in performance between these methodologies. The fraction of Trues after the θ and E_c filters are 0.541 and 0.837, respectively. This information is summarized in Tab. III.

The variance in the Random contamination rate explains the difference in enhancement observed in Fig. 2. Applying both filters greatly mitigated Random leakage (only 5 of the 2.72×10^6 survived), though the surviving Trues were also reduced with this strengthening criteria, with 4,012 (0.00148%) of 2.72×10^6 surviving.

DISCUSSION

This study aimed to assess the viability of utilizing QE-information in improving event classification within a combined PET-Compton Camera (PET-CC) system in which both β^+ and prompt gamma emissions were expected – particularly in distinguishing true positron annihilation events from Random events caused by prompt gamma contamination. Our quantitative analysis based on Monte

Tab. III. Of the 5.43 ×10⁶ DCSc, the portion of the data which falls within the QE-selection criteria for presented filters.

APPLIED FILTER			
10%	$\theta \in [73.12, 91.68]°$	Ec ∈ 235 ±	keV
Both	6,249	1,293	5
True		0.837	0.99876
Count 7,381 6,646 4,012			
Random Count			
True Fraction 0.541			

Carlo simulation highlighted several key insights into the potential and limitations of using QE to refine event sorting and enhance imaging performance.

The results indicate that the overall sensitivity of the system greatly favors those in which the initial interaction of any photon is Compton scattering. The standard PET cases (sum of case 1, 2, and 10) afforded a sensitivity of 0.562%. The addition of case 7 alone (miss, miss, C), representing Compton camera mode sensitivity, increased overall system sensitivity by 12.304 percentage points. However, many of these cases intrinsically contain ambiguity in event pairing, which must be addressed. The presence of energy ambiguity, particularly in Case 3, underscores the challenge of accurately pairing annihilation photons when γ_{Prompt} deposits energy similar to that of γ_{Ann}. The total sensitivity of 1.995% for case 3 suggests a significant potential for QE information to aid (note, aid, not solely resolve) in addressing these ambiguities. We show that the information-basis used in selecting the subset of data with greatest QE sensitivity matters. Unfiltered data exhibited a weak $\Delta\phi$ dependence, with R ≈ 1.15, indicating that, without any filtering, the mixed data set (comprising both true and random events), offers limited potential for QE to enhance event classification. Applying filters based on polar scattering angles (θ) and the energy of the initial Compton scatter (E_C) revealed the nuanced behavior of computing scattering kinematics. The θ - based filter resulted in a mixed data set, with R ≈ 1.4, significantly lower than the R ≈ 2.25 observed for true data alone. This discrepancy is due to the inclusion of a higher proportion of Random events within the θ window, which may scatter within the defined angle range by chance, rather than due to genuine Compton kinematics.

In contrast, filtering based on E_C yielded a higher enhancement ratio of R ≈ 1.8. This result suggests that energy-based filtering more effectively discriminates between True and Random events, likely because Random events cannot replicate the specific energy deposition patterns of true annihilation photon coincidence events. The ability of the E_C filter to more accurately select for true QE events points to its potential utility in improving the accuracy of event classification in PET-CC systems. This finding is supported by the True fraction in the postfilter data: 0.541 *vs.* 0.837 for the θ and E_C filters, respectively.

While the application of QE has shown promise in enhancing event classification of $\beta^+\gamma$ coincidences, the findings also underscore several limitations. The relatively low enhancement ratios in mixed data sets suggest that while QE can improve classification, it may not be sufficient on its own to fully resolve all ambiguities, particularly in cases with significant γ_{Prompt} contamination. Moreover, the variation in performance between different filtering strategies highlights the need for further refinement of the criteria to best leverage QE-information.

Future work should explore the development of more sophisticated filtering algorithms that can dynamically adjust to the specific characteristics of the detected events. Further research should also investigate the impact of QE on multi-isotope studies, in which accurate event classification is particularly challenging.

CONCLUSIONS

This study demonstrated the potential of utilizing QE-information to enhance event classification within a combined PET-Compton Camera system for an isotope with dual β^+ and γ_{Prompt} emission. Our findings show that a significant portion of the possible $\beta^+\gamma$ coincidence cases contain the potential for energy ambiguity between the a γ_{Prompt} and γ_{Ann}, and further that a set of these are targetable with QE methods. Filtering based on the energy of the initial Compton scatter proved more effective in enhancing QE--dependent event classification compared to polar angle filtering with only slight loss to True sensitivity. However, the relatively modest enhancement ratios in mixed data sets indicate that further refinement of filtering algorithms is necessary. Future work should focus on developing dynamic filtering techniques and expanding the investigation to multi-isotope studies, where accurate event classification remains a significant challenge.

CONFLICT OF INTEREST

Authors have declared no potential conflicts of interest.

REFERENCES

1. Beekman FJ, Kamphuis C, Koustoulidou S, Ramakers RM, Goorden MC. Positron range-free and multi-isotope tomography of positron emitters. Phys Med Biol. 2021;66:065011.
2. Llosá G, Rafecas M. Hybrid PET/Compton-camera imaging: An imager for the next generation. Eur Phys J Plus. 2023;138(3):214.
3. Pratt EC, Lopez-Montes A, Volpe A, Crowley MJ, Carter LM, Mittal V, et al. Simultaneous quantitative imaging of two PET radiotracers via the detection of positron–electron annihilation and prompt gamma emissions. Nat Biomed Eng. 2023;7(8):1028–39.
4. Shimazoe K, Uenomachi M. Multi-molecule imaging and inter-molecular imaging in nuclear medicine. Bio-Algorithms Med Systems. 2022;18(1):127–34.
5. Beyene EY, Das M, Durak-Kozica M, Korcyl G, Mryka W, Niedźwiecki S, et al. Exploration of simultaneous dual-isotope imaging with multi-photon modular J-PET scanner. Bio-Algorithms Med Systems. 2023;19(1):101–8.
6. Moskal P, Baran J, Bass S, Choiński J, Chug N, Curceanu C, et al. Positronium image of the human brain in vivo. Sci Adv. 2024;10(37):eadp2840.
7. Moskal P, Dulski K, Chug N, Curceanu C, Czerwiński E, Dadgar M, et al. Positronium imaging with the novel multiphoton PET scanner. Sci Adv. 2021;7(42):eabh4394.
8. Yoshida E, Tashima H, Nagatsu K, Tsuji AB, Kamada K, Parodi K, et al. Whole gamma imaging: A new concept of PET combined with Compton imaging. Phys Med Biol. 2020;65(12):125013.
9. Manzano LG, Abaline JM, Acounis S, Beaupère N, Beney JL, Bert J, et al. XEMIS2: A liquid xenon detector for small animal medical imaging. Nucl Instrum Methods Phys Res A. 2018;912:329–32.
10. Shoop G, Abbaszadeh S. Combining PET and Compton imaging with edge-on CZT detectors for enhanced diagnostic capabilities. Adv Radiother Nucl Med. 2024;2(2):3330.
11. Pryce MHL, Ward JC. Angular correlation effects with annihilation radiation. Nature. 1947;160:435–35.
12. Snyder HS, Pasternack S, Hornbostel J. Angular correlation of scattered annihilation radiation. Phys Rev. 1948;73:440–8.
13. Bohm D, Aharonov Y. Discussion of experimental proof for the paradox of Einstein, Rosen, and Podolsky. Phys Rev. 1957;108:1070–6.
14. Moskal P. Towards total-body modular PET for positronium and quantum entanglement imaging. In: IEEE 2018: 2018 IEEE Nuclear Science Symposium and Medical Imaging Conference Proceedings (NSS/MIC); 2018 Nov 10-17; New York: IEEE. p. 1–4.
15. Caradonna P, Reutens D, Takahashi T, Takeda S, Vegh V. Probing entanglement in Compton interactions. J Phys Commun. 2019;3:105005.
16. Watts DP, Bordes J, Brown JR, Cherlin A, Newton R, Allison J, et al. Photon quantum entanglement in the MeV regime and its application in PET imaging. Nat Commun. 2021;12:2646.
17. Strizhak A, Abdurashitov D, Baranov A, Ivashkin A, Musin S. Study of the Compton scattering of entangled annihilation photons. Phys Part Nuclei Lett. 2022;19:509–12.
18. Abdurashitov D, Baranov A, Borisenko D, Guber F, Ivashkin A, Morozov S, et al. Setup of Compton polarimeters for measuring entangled annihilation photons. J Inst. 2022;17:P03010.
19. Ivashkin A, Abdurashitov D, Baranov A, Guber F, Morozov S, Musin S, et al. Testing entanglement of annihilation photons. Sci Rep. 2023;13:7559.
20. Moskal P, Kumar D, Sharma S, Beyene EY, Chug N, Coussat A, et al. Non-maximal entanglement of photons from positron-electron annihilation demonstrated using a novel plastic PET scanner. arXiv preprint arXiv:2407.08574.2024.
21. Parashari S, Bosnar D, Friščić I, Kožuljević AM, Kuncic Z, Žugec P, et al. Closing the door on the "puzzle of decoherence" of annihilation quanta. Phys Lett B. 2024;852:138628.
22. Tkachev I, Musin S, Abdurashitov D, Baranov A, Guber F, Ivashkin A, et al. Measuring the evolution of entanglement in Compton scattering. arXiv preprint arXiv:2406.14352.2024.
23. Bordes J, Brown JR, Watts DP, Bashkanov M, Gibson K, Newton R, et al. First detailed study of the quantum decoherence of entangled gamma photons. Phys Rev Lett. 2024;133(13):132502.
24. Caradonna P. Kinematic analysis of multiple Compton scattering in quantum-entangled two-photon systems. Ann Phys. 2024;470:169779.
25. Jan S, Santin G, Strul D, Staelens S, Assié K, Autret D, et al. GATE: A simulation toolkit for PET and SPECT. Phys Med Biol. 2004;49(19):4543–61.
26. Agostinelli S, Allison J, Amako K, Apostolakis J, Araujo H, Arce P, et al. GEANT4 – a simulation toolkit. Nucl Instrum Methods Phys Res A. 2003;506(3):250–303.
27. Perkins ST, Cullen DE, Chen MH, Rathkopf J, Scofield J, Hubbell JH. Tables and graphs of atomic subshell and relaxation data derived from the LLNL Evaluated Atomic Data Library (EADL), Z= 1–100. Lawrence Livermore National Laboratory; 1991 July. Report No.: UCRL-50400-Vol. 30.
28. Romanchek G, Shoop G, Gholami K, Enlow E, Abbaszadeh S. Quantum entanglement filtering: A PET feasibility study in imaging dual-positron and prompt gamma emission via Monte Carlo simulation. IEEE Trans Radiat Plasma Med Sci. 2024;8(8):916–25.
29. Li M, Yockey B, Abbaszadeh S. Design study of a dedicated head and neck cancer PET system. IEEE Trans Radiat Plasma Med Sci. 2020;4(4):489–97.
30. Wang Y, Herbst R, Abbaszadeh S. Development and characterization of modular readout design for two-panel head-and-neck dedicated PET system based on CZT detectors. IEEE Trans Radiat Plasma Med Sci. 2021;6(5):517–21.
31. Enlow E, Diba M, Clayton J, Harris B, Abbaszadeh S. Impact of flexible circuit bonding and system integration on energy resolution of cross-strip CZT detectors. IEEE Trans Radiat Plasma Med Sci. 2023 Mar 22;7(6):580–6.
32. Gu Y, Levin CS. Study of electrode pattern design for a CZT-based PET detector. Phys Med Biol. 2014;59(11):2599.
33. Abbaszadeh S, Chinn G, Levin CS. Positioning true coincidences that undergo inter-and intra-crystal scatter for a sub-mm resolution cadmium zinc telluride-based PET system. Phys Med Biol. 2018;63(2):025012.